INTERFACE

royalsocietypublishing.org/journal/rsif

Research

Cite this article: Tsai L, Navarro P, Wu S, Levinson T, Mendoza E, Janneke Schwaner M, Daley MA, Azizi E, Ilton M. 2024 Viscoelastic materials are most energy efficient when loaded and unloaded at equal rates. *J. R. Soc. Interface* **21**: 20230527.
https://doi.org/10.1098/rsif.2023.0527

Received: 11 September 2023
Accepted: 4 January 2024

Subject Category:
Life Sciences–Physics interface

Subject Areas:
biomaterials, biomechanics

Keywords:
tendon, resilience, viscoelasticity, biological spring

Author for correspondence:
Mark Ilton
e-mail: milton@g.hmc.edu

Electronic supplementary material is available online at https://doi.org/10.6084/m9.figshare.c.7029148.

THE ROYAL SOCIETY PUBLISHING

Viscoelastic materials are most energy efficient when loaded and unloaded at equal rates

Lucien Tsai[1], Paco Navarro[1], Siqi Wu[1], Taylor Levinson[1], Elizabeth Mendoza[2], M. Janneke Schwaner[2], Monica A. Daley[2], Emanuel Azizi[2] and Mark Ilton[1]

[1]Department of Physics, Harvey Mudd College, Claremont, CA 91711, USA
[2]Department of Ecology and Evolutionary Biology, University of California, Irvine, CA 92697, USA

MAD, 0000-0001-8584-2052; MI, 0000-0002-2439-3940

Biological springs can be used in nature for energy conservation and ultra-fast motion. The loading and unloading rates of elastic materials can play an important role in determining how the properties of these springs affect movements. We investigate the mechanical energy efficiency of biological springs (American bullfrog plantaris tendons and guinea fowl lateral gastrocnemius tendons) and synthetic elastomers. We measure these materials under symmetric rates (equal loading and unloading durations) and asymmetric rates (unequal loading and unloading durations) using novel dynamic mechanical analysis measurements. We find that mechanical efficiency is highest at symmetric rates and significantly decreases with a larger degree of asymmetry. A generalized one-dimensional Maxwell model with no fitting parameters captures the experimental results based on the independently characterized linear viscoelastic properties of the materials. The model further shows that a broader viscoelastic relaxation spectrum enhances the effect of rate-asymmetry on efficiency. Overall, our study provides valuable insights into the interplay between material properties and unloading dynamics in both biological and synthetic elastic systems.

1. Introduction

Biological springs perform a variety of functions in natural movements including energy conservation and latch-mediated spring actuation [1–4]. Energy-conserving movements involve cyclic, repeating locomotor patterns such as terrestrial running or hopping gaits [5–7], insect flight [8,9] and fish swimming [10]. By contrast, latch-mediated spring actuation is characterized by a rapid release of energy such as the movements of jumping frogs [11,12] and insects [13–16], raptorial appendage strikes of mantis shrimps [17,18], tongue projections of chameleons [19–21] and mandible closures of trap-jaw ants [22]. These diverse functions often result in variations in the relative rate of loading and unloading of elastic structures during a movement. Elastic structures used for latch-mediated spring actuation are often loaded at slow rates compared with the rapid unloading rates associated with elastic recoil (figure 1*a*). By contrast, the behaviour of elastic structures during cyclic movements are more varied. Previous work has shown symmetrical patterns with near equal strain rates observed during loading and unloading [25]. Others have shown that tendon strain rates are highest during loading, at the beginning of the stance phase (figure 1*b*). The diverse patterns of loading and unloading rates observed in biological systems suggest that shifts in mechanical properties arising from rate-asymmetry are likely to have significant performance consequences.

For vertebrates, tendon is a tissue often characterized as a biological spring that operates in series with skeletal muscle [1] and exhibits a highly nonlinear elastic response. When stretched, tendon is relatively compliant at low strain and stiffens before reaching a roughly linear elastic regime at approximately 3–10% strain [26]. This strain-stiffening response enables significant elastic

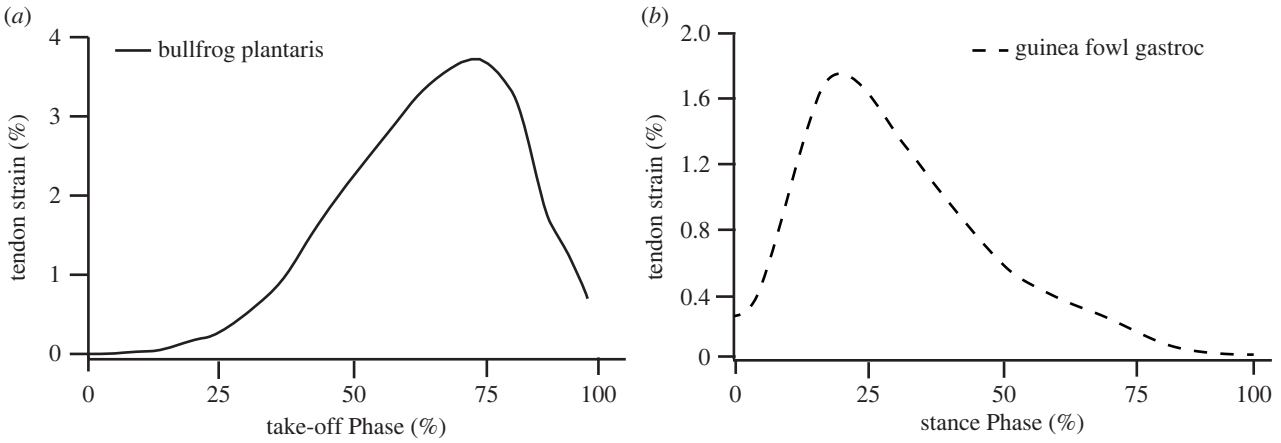

Figure 1. Strains patterns experienced by tendons *in vivo* during latch-mediated spring actuation (*a*) and cyclic locomotion (*b*). (*a*) Tendon strains in the plantaris (gastrocnemius) tendon of bullfrogs plotted against the proportion of the take-off phase of a single representative jump. The maximum strain rate during the unloading phase is approximately 3.5 times faster than the loading phase. (*b*) Strain of the lateral gastrocnemius tendon of guinea fowl during the stance phase of a representative running trial. The maximum tendon strain rates experienced during the loading are faster that those observed during the unloading phase. These plots highlight the variation in observed strain patterns during different modes of locomotion. Data for (*a*) and (*b*) are recreated from [23,24], respectively.

energy storage in tendon to drive latch-mediated spring-actuated movements [11,12,27]. Tendons also operate with relatively high mechanical energy efficiency which allows them to conserve energy during cyclical movements [1,25].

Previous work on the mechanical energy efficiency of tendons has focused on symmetric loading and unloading rates. The primary metric used to describe a material's energy efficiency is its resilience, defined as the ratio of the energy released divided by the energy stored during a single loading and unloading cycle. Tendon has been shown to have a 90–95% resilience over a range of symmetric rates (approx. 0.1 to 10 Hz) [28–30] with a range of resilience from 80% to 97% measured across a variety of tendons [31]. However, resilience can depend on how it is measured. For example, when measured as a mass–spring system, tendons from the feet of sheep have a significantly lower resilience (62% at 5 Hz) [32].

Although the literature has historically focused on tendon stretched at symmetric rates, the growing body of literature suggests that tendons undergo diverse patterns of asymmetric loading rates during natural behaviours (figure 1). These observed differences in loading and unloading rates have motivated studies to explore the response to asymmetric rates in tendon [30] and other biological springs [33] over a relatively narrow range of asymmetry.

Here, we explore rate-asymmetry over a broad range of timescales to understand its underlying physical principles. In this study, we ask: is there a connection between the biological function of energy-conserving movements and material performance under symmetric rates? How does changing the relative loading and unloading rate affect the mechanical efficiency of tendon? The measurement of materials at asymmetric rates is typically performed using elastic recoil experiments, where a material is slowly loaded followed by a rapid high-rate unloading of elastic waves in the material [34–42]; however, these measurements require strains larger than those accessible with tendon.

To address these guiding questions in tendons, we perform novel dynamic mechanical analysis (DMA) measurements using triangular waveforms that either have the same loading and unloading times (symmetric rates) or different loading and unloading times (asymmetric rates) for the same maximum strain. By measuring lateral gastrocnemius tendons from guinea fowl and plantaris tendons from American bullfrogs, we find these tendons are most energy efficient when subjected to symmetric loading and unloading rates. To test the generality of this result and understand its underlying physical cause, we also repeat the same measurements on synthetic elastomer materials with known linear viscoelastic properties and perform simulations. We find the same qualitative result independent of the material and amount of applied deformation: a higher degree of asymmetry between the loading and unloading rates reduces mechanical energy efficiency. Using a one-dimensional linear viscoelastic model, we find that a broad distribution of relaxation times (characteristic of biological materials) enhances the strength of the asymmetric rate effect. Given the generality of our model and results, these findings should be applicable to a wide range of biological materials and could be used to inform the design of efficient elastic mechanisms in soft robotics and bioengineering.

2. Results

We measured the mechanical response of American bullfrog plantaris tendons (used to drive rapid motion during jumping) and guinea fowl lateral gastrocnemius tendons (used in walking and running). We stretched the tendons by increasing their length by 5% and returning them back to their original length at controlled loading and unloading rates (figure 2*a*,*b*). For equal loading and unloading rates, the tendons returned approximately 80% of the mechanical energy applied during stretching with a slight increase in resilience as the symmetric loading/unloading time increased (towards the upper-right in both figure 2*c*,*d*). For asymmetric rates, we either applied a slow loading followed by a fast unloading or vice versa. For the most extreme differences between the loading and unloading rates we measured, the resilience decreased of both types of tendons significantly to approximately 60% (figure 2*c*,*d*). Given a fixed loading rate, we found that the maximum resilience generally occurs when the unloading rate matches the loading rate.

To understand the generality and the underlying physical principles of this phenomenon, we performed similar

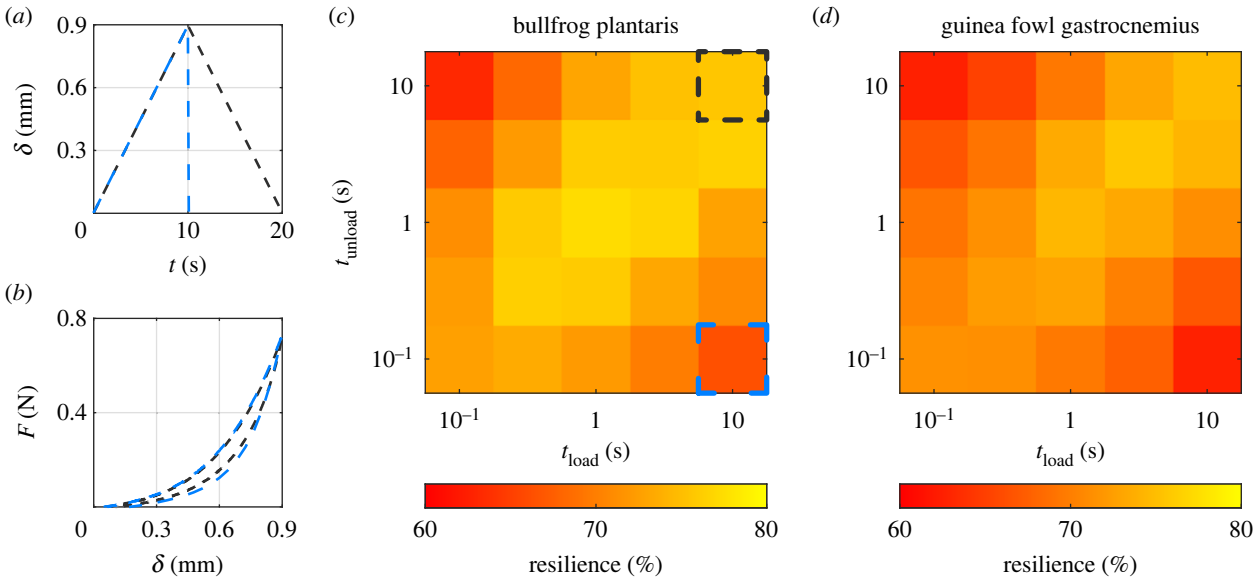

Figure 2. Tendons are most mechanically efficient when loaded and unloaded at equal rates. (*a*) The displacement–time (δ–t) profiles for a symmetric rate test where a tendon was loaded for 10 s and unloaded for 10 s (dashed black curve) and an asymmetric rate test where the tendon was loaded for 10 s and unloaded for 0.1 s (dashed blue curve). (*b*) Representative force–displacement (F–δ) responses of bullfrog plantaris tendon to the two displacement-time inputs from (*a*). The tendons exhibit a characteristic strain-stiffening response with a low hysteresis between the loading and unloading curves (high resilience). The tendon has a lower resilience for the asymmetric rate (dashed blue curve) compared with the symmetric rate (dashed black curve). (*c*) The resilience of bullfrog plantaris tendons was measured for different combinations of loading and unloading rates. The resilience was highest when measured at symmetric rates, which corresponds to the diagonal elements of the heatmap. Each resilience is calculated from an average of five tendons. The black and blue dashed squares indicate the rates described in (*a*) and (*b*). (*d*) The average resilience of five guinea fowl lateral gastrocnemius tendons was consistent with the bullfrog plantaris tendon response. The full dataset is available in electronic supplementary material, tables S1 and S2.

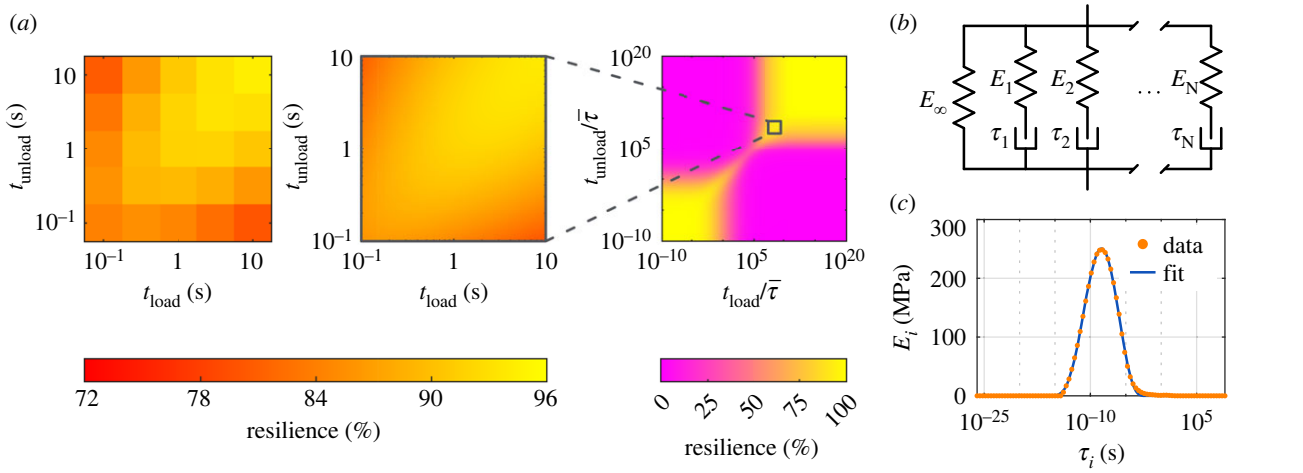

Figure 3. Symmetric loading and unloading rates are also most mechanically efficient for a synthetic polyurethane elastomer. (*a*) The experimentally measured average resilience of six polyurethane elastomer samples (left) and its simulated resilience (middle) both show a significant decrease when the loading and unloading rates are unequal. The resilience for the experimental timescales used (left and middle panels) is a part of a larger resilience profile (right) normalized by the mean characteristic relaxation time $\bar{\tau}$. The experimental timescales within this larger profile is denoted by the grey box and lies near the edge of the backbone region (yellow diagonal). (*b*) The simulations were performed using a generalized Maxwell solid model. The single spring E_∞ represents the long-time equilibrium behaviour of the solid, while each pair of spring and dashpot in series (E_i, τ_i) represent a characteristic relaxation modulus and timescale in the material. (*c*) An E_∞ of 28.2 MPa and the values for $N = 90$ E_i, τ_i pairs (orange dots) for the spring-damper elements are obtained from a one-dimensional linear viscoelastic characterization of the polyurethane elastomer. A Pearson distribution (blue curve) was fitted to the discrete relaxation spectrum to create a continuous representation of the spectrum.

measurements on synthetic elastomers. The synthetic elastomers enable us to measure their viscoelastic properties in the linear regime using time-temperature superposition that includes measurements on samples at sub-freezing temperatures, conditions which are inaccessible to the tendon samples without causing changes to the mechanical response of the tissue.

Synthetic elastomer materials exhibit the same response as tendon to rate-asymmetry: they are most mechanically efficient when the loading and unloading rates are equal. The resilience of the polyurethane elastomer at a 1% maximum strain (left panel of figure 3*a*) was found to be relatively high with symmetric rates (greater than 90%), but had an approximately 20% drop in resilience over the two orders of

magnitude in asymmetry measured. At higher maximum strains where nonlinear effects are more pronounced, the polyurethane elastomer showed a similar significant decrease in resilience with more asymmetry and was slightly less resilient overall (electronic supplementary material, figure S3). A more dissipative elastomer, neoprene, was also consistent with this result (electronic supplementary material, figure S4).

To understand why materials are less energy efficient when subjected to asymmetric rates, we used the one-dimensional generalized Maxwell model, a discrete linear viscoelastic representation of solids (figure 3*b*). The model consists of an elastic element that accounts for the long-term equilibrium mechanical response of the material (E_∞) in parallel with elastic and viscous (spring and dashpot) elements that each confer a stiffness and characteristic relaxation time (E_i and τ_i for $i = 1, \ldots, N$). We measured the linear viscoelastic response of the polyurethane elastomer using time-temperature superposition to obtain values for E_∞ (28.2 MPa) and the discrete relaxation spectrum of E_i versus τ_i (orange dots in figure 3*c*) that we use to simulate the material response to symmetric and asymmetric loading and unloading rates. From this one-dimensional linear viscoelastic model, the simulated resilience values are independent of the maximum strain (electronic supplementary material: Independence from $\epsilon_{\max}$) and the modulus dependence is solely based on E_0/E_∞, the ratio of the instantaneous modulus ($E_0 = E_\infty + \sum E_i$) to the equilibrium modulus (E_∞), with a higher E_0/E_∞ value corresponding to a more dissipative viscoelastic material (electronic supplementary material: Dependence on E_0/E_∞).

To validate our modelling approach, we compared the simulated resilience with the measured resilience of the polyurethane elastomer under the same stretching conditions for the range of loading and unloading times tested. The simulated resilience shows an excellent agreement with the experimentally measured data (left and middle panels of figure 3*a*) with a less than 2% difference in resilience between the experiment and simulation (electronic supplementary material, figure S2). This agreement between the experiment and simulation demonstrates that a simple one-dimensional linear viscoelastic model captures the important mechanical properties necessary to reproduce the reduced efficiency at asymmetric rates.

Using the discrete relaxation spectrum and E_∞ for the polyurethane elastomer, the resilience at timescales beyond the experimental loading/unloading times was simulated (right panel of figure 3*a*) to capture the full resilience profile. We find regions of high resilience (yellow squares in the right panel of figure 3*a*) for very short timescales (fast rates) and very long timescales (slow rates) relative to the mean characteristic relaxation time of the material $\bar{\tau}$. For the short timescale, none of the dissipative modes become active as long as $t_{\text{load}} \ll \bar{\tau}$ and $t_{\text{unload}} \ll \bar{\tau}$. For long timescales, the system is adiabatic and energy is approximately conserved in the material if $t_{\text{load}} \gg \bar{\tau}$ and $t_{\text{unload}} \gg \bar{\tau}$. In addition, we find a backbone region (the edge of which the experimental window is located) joining these extremes where the loading and unloading rates must closely match to have a high resilience (yellow diagonal in the right panel of figure 3*a*). In the regions not covered by the extremes, a higher degree of asymmetry results in a lower resilience (pink areas in the right panel of figure 3*a*).

These regions of higher resilience do not necessarily correspond to a higher overall energy output. For short unloading times, the highest energy output occurs when the loading time is also short (electronic supplementary material, figure S5), and the overall energy output of fast unloading decreases significantly when the loading time is increased (electronic supplementary material, figure S5b). The elastic energy output can also be significantly modulated by changing the applied strain, or by changing the overall volume of elastic material. Because these factors are highly variable across different elastic systems, we focus on resilience rather than energy output in this work.

With the modelling approach validated, we further use a one-dimensional linear viscoelastic model to explore how resilience depends on material properties over a broad range of loading and unloading rates. To reduce the number of parameters in our model, we represent the discrete relaxation spectrum as a continuous curve and fit a Pearson distribution on a $\log \tau$ scale (blue curve of figure 3*c*). This fit depends on only four parameters: a mean of $\log \bar{\tau} = -8.56$, standard deviation of $\log \sigma = 2.05$, skewness of $\gamma_1 = -0.0847$ and kurtosis of $\beta_2 = 2.55$ (with $\gamma_1 = 0$ and $\beta_2 = 3$ for a normal distribution). We use this continuous relaxation spectrum (blue curve of figure 3*c*) with $N = 10^3$ discrete points (E_i, τ_i) chosen equally spaced on the $\log \tau$ scale and the corresponding E_0/E_∞ value of 126 to match the polyurethane elastomer's linear viscoelastic properties as a starting point for the simulations. We find two primary properties of the material that shape the resilience response to asymmetric rates: (i) the ratio between the instantaneous modulus E_0 and the equilibrium modulus E_∞ and (ii) the breadth of the material's relaxation spectrum characterized by the standard deviation $\log \sigma$.

To explore how changes in E_0 relative to E_∞ change the resilience, we compared the resilience profile of different E_0/E_∞ values represented by a change in the height of the continuous relaxation spectrum with a constant E_∞ (figure 4*a*). At the short and long timescale extremes characteristic of high resilience (yellow squares in the panels of figure 4*b*), we find that E_0/E_∞ does not significantly affect the resilience. By contrast, the resilience is significantly impacted by E_0/E_∞ in the regions of low resilience, asymmetric stretching (orange areas in the left panel to pink areas in the right panel of figure 4*b*) with a lower resilience for larger values of E_0/E_∞. The resilience in these regions converges to $E_\infty/E_0 \times 100\%$ as the loading and unloading rates become more asymmetric.

Using the model, we also examined how changes to the distribution of the relaxation spectrum affect how a material responds to rate-asymmetry. By varying $\log \sigma$, we find that the breadth of the relaxation spectrum affects the resilience profile (figure 5). For a material with a narrow distribution of relaxation times, the material is highly resilient if the loading and unloading times both occur on the very short or very long timescale extremes (left panel of figure 5*b*). In these regions, the resilience is high even if the loading and unloading rates are quite different (yellow squares in the left panel of figure 5*b*). However, for a broader relaxation spectrum, the resilience is high when the loading and unloading rates match, regardless of the experimental timescale (yellow diagonal in the right panel of figure 5*b*). Thus, the breadth of the viscoelastic relaxation spectrum is important in shaping how the mechanical efficiency of the material responds to asymmetric rates. We also examined higher-order moments of the relaxation spectrum and found no significant changes with varying skewness (electronic supplementary material, figure S6) while a higher kurtosis broadens the resilience

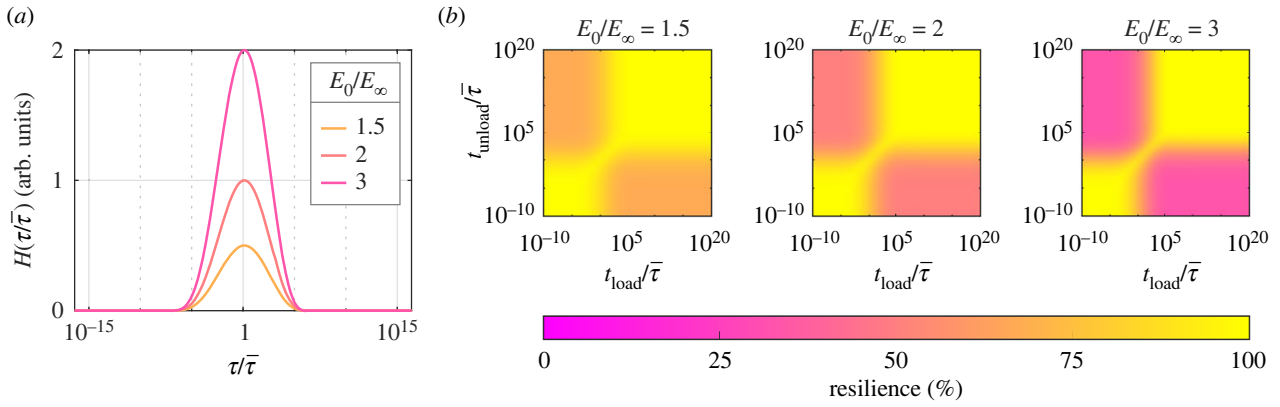

Figure 4. A more dissipative viscoelastic material has a lower resilience at asymmetric rates. (*a*) Using the generalized Maxwell model, E_0/E_∞ was varied from the experimental value of $E_0/E_\infty = 126$. (*b*) A larger value of E_0/E_∞ (left to right on the panels), constituting a larger stiffness contribution from the spring-dashpot elements $\sum E_i$ compared with the long-term equilibrium spring E_∞, lowers the resilience in the regions significantly impacted by asymmetric stretching (orange areas in left panel to pink areas in right panel) with the resilience converging to $E_\infty/E_0 \times 100\%$ as the rate-asymmetry is increased. The resilience at the extremes (t_{load}, $t_{unload} << \bar{\tau}$ and t_{load}, $t_{unload} >> \bar{\tau}$) depicted by the yellow squares is not significantly affected and remains at nearly 100% resilience.

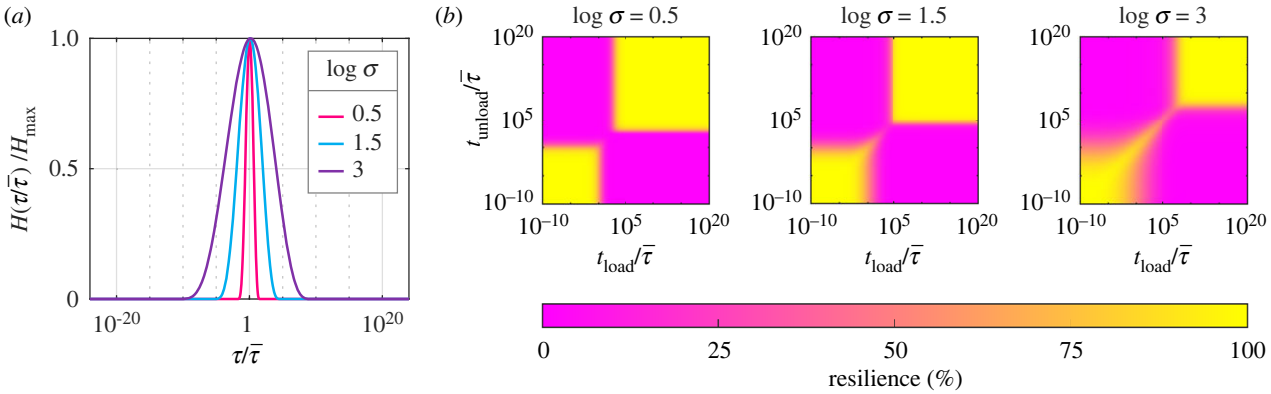

Figure 5. A broader viscoelastic relaxation spectrum increases the impact of rate-asymmetry on resilience. (*a*) Using the generalized Maxwell model, we compare the effect of increasing the breadth of the relaxation spectrum by varying the standard deviation from the experimental value of $\log \sigma = 2.05$. (*b*) For a narrow relaxation spectrum (left panel), the material is resilient if both the loading and unloading rates are much slower or are both much faster than the mean characteristic relaxation time $\bar{\tau}$. For a broader relaxation spectrum (right panel), the loading and unloading rates need to closely match to have a high resilience.

transition between the long timescale extreme and asymmetric regions (electronic supplementary material, figure S7).

Finally, we verified the generality of the results to asymmetric loading and unloading conditions with non-constant rates. In the *in vivo* tendon measurements (figure 1), the strain rate during each phase of movement is not constant. To explore this effect, we calculated the resilience for piecewise smooth sinusoidal strain loading and unloading profiles. The calculated resilience yields the same main result: over a broad range of rates, viscoelastic materials recover elastic energy most efficiently when the loading and unloading rates match (electronic supplementary material, figure S8). In this work, although we performed the calculations using only two functional forms for the strain profile (constant rate and piecewise sinusoidal), these functional forms are extremely different in how abruptly they transition from loading to unloading. We therefore believe that our results will hold for any arbitrary strain profile, with a more rigorous analysis needed to prove full generality.

3. Discussion

Using a combination of experimental mechanical properties measurements and continuum material modelling, we find that viscoelastic materials are most mechanically efficient when loaded and unloaded at the same rate. The breadth of a material's viscoelastic relaxation spectrum is a key factor that determines the extent to which it will exhibit a drop in efficiency in response to asymmetric loading and unloading rates. Given the generality of our approach, we expect these results to apply to a variety of materials used in elastically driven movements in biology such as resilin-rich cuticle in locusts [15] or chitinous exoskeleton used by mantis shrimp [18] as well as the actuation of soft elastomers in recent robotics applications [43,44].

For biological materials with a broad distribution of relaxation times, various levels of the hierarchical material structure could respond differently to asymmetry in the loading and unloading rates. The materials that comprise biological springs are often composite materials that yield a complex mechanical response to deformation [45,46]. Biological materials have a multi-scale hierarchical structure that causes multiple important length scales and timescales to emerge in response to mechanical deformation [47–50]. This hierarchical structure results in a broad viscoelastic relaxation spectrum caused by the different dynamical properties at the individual protein level [47] and at the whole tissue level [49,50].

In our measurements here, we are operating at the tissue level and see pronounced differences with an

approximately 20% drop in resilience at asymmetric rates. At the next level down from the whole tissue, tendons comprise tendon fascicles. Rosario & Roberts examined the mechanical properties of rat tail tendon fascicles and observed no dependence on rate-asymmetry [30]. This suggests that perhaps the important broadening of the relaxation spectrum of tendon for its rate-asymmetric behaviour occurs at the tissue level. However, there are some important limitations to this comparison. The fascicle measurements were performed at close to symmetric rates (only a factor of 0.5–4× difference in loading/unloading rate), the lower forces of fascicles yielded noisier data, and there are functional differences between rat tail tendon and the energy storing tendons we examined in this work. Future work comparing the relaxation spectrum across multiple levels of biological material structure would provide insight into the emergence of rate-asymmetry. Structural differences found in energy storing versus positional tendons [51] may also reveal differences in the rate-asymmetric response of tendons.

Our results here also have potential impact in comparative biomechanics. Previous work has highlighted how strain rate can affect functional traits of biomechanical systems [52]. Translating our results here into the language of [52]: the viscoelastic relaxation spectrum of the tendon (functional trait) determines the tendon's resilience (attribute) based on the loading/unloading rate of the material (external factor). Future work could probe deeper into this structure–property relationship of tendon. Previous work has demonstrated there are morphological changes that correlate to changes in external factors or overall function [53–55]. Our work here provides a framework for future investigation into these morphological changes. Measuring specific properties of the viscoelastic functional trait of biological materials (specifically E_0/E_∞ and the breadth of the spectrum) determines how efficiently they will respond to a variety of external loading factors. Therefore, connecting changes in morphology to these specific properties could inform the analysis of form–function relationships in biomechanical systems.

In animals that use latch-mediated spring actuation, muscles cannot load elastic energy quickly enough to match the unloading rates, otherwise the elastic structure would not be required to have a high kinematic output. However, there is some evidence that these timescales are not on the extremes of asymmetry (e.g. smasher mantis shrimp still load at 300 ms even though they could take longer because of their slow-moving prey) [56]. Why don't these animals use slower muscle contractions to load their elastic mechanisms? From our work here, we see there would be no energetic benefit to loading more slowly. A slower loading would increase the rate-asymmetry and thus decrease the resilience of the elastic materials. For a short unloading time like those characteristic of ultra-fast movements, a shorter loading time actually yields an overall higher energy output (electronic supplementary material, figure S5) due to stress-relaxation that occurs during a slow loading.

Biological springs are also used for damping and deceleration (power attenuation) in landing and declined running movements [1,57,58]. The performance of elastic structures in biomechanics will often need to balance multiple roles, such as balancing energy conservation and damping in passive elastic movements found in cockroach legs [59]. Our work here suggests that viscoelastic materials will have a similar energy efficiency when used during power attenuating movements (fast loading followed by a slow unloading) compared with latch-mediated spring actuation movements (slow loading followed by fast unloading). Future work measuring the asymmetric rate response of biological materials that balance different functional roles might uncover interesting distinctions between them.

Our work suggests that symmetric loading and unloading rates are the most mechanically efficient, but gaits that involve cyclic loading and unloading can be biased towards a shorter loading time. For example, asymmetric ground reaction forces have been observed in running birds and lizards, with the loading phase occurring more rapidly than unloading [60–62]. This asymmetric gait appears to be more pronounced among animals that have a body centre of mass (CoM) positioned forward of the hip [62]. However, humans also exhibit asymmetry in the elastic bounce of the leg and body, observed in ground reaction forces and body CoM motion, but the asymmetry decreases with increasing speed [63,64]. Models that include intrinsic damping in the leg with a single characteristic relaxation time predict these asymmetric gaits are energetically optimal [61]. But our results here suggest that a broad spectrum of relaxation times could be important for the emergence of symmetric rate efficiency, and biomechanical models that incorporate a more realistic viscoelastic model could uncover shifts in energetically optimal gaits.

There are some important limitations in the scope of this work. Although here we focused on the efficiency of energy released from elastic structures, there are other behavioural and physiological factors that contribute to the relative loading and unloading rates of elastic biomechanical systems. The dynamics of the entire biomechanical system contribute to the overall performance, with muscle properties, linkage mechanics and load mass all being important for the kinematics of fast elastic movements [3]. Energy can be lost during muscle contractions and to the environment, and there are multiple ways that animals minimize the energetic cost of locomotion. For example, changing gait and muscle activation patterns during running can help minimize losses during ground contact [65,66] and increase efficiency during incline running [60].

Other limitations in the work include simplifications made in the model. We used a one-dimensional linear viscoelastic model as a minimal model to capture the essential features of the asymmetric rate effect. But there are multiaxial stress states and nonlinear viscoelasticity in tendons [67]. We also considered tendons and synthetic viscoelastic materials of a relatively similar size, but the size-scale of the elastic material can also be an important consideration when assessing its kinematic performance [39]. At small size-scales, viscous drag forces can significantly impede locomotion [68] and can be a significant source of dissipation for fast elastic movements [69]. These additional effects could be added to extend the model and further generalize the results of this work.

4. Conclusion

In this study, we examined the mechanical energy efficiency of biological springs and synthetic materials under symmetric and asymmetric loading/unloading rates. Our results reveal that these materials are most mechanically efficient when

subjected to symmetric loading and unloading rates. This finding holds true for both tendons and synthetic elastomers. By using a one-dimensional linear viscoelastic model to analyse the data, we gained insight into the underlying principles governing the resilience of these materials. We found that the ratio between the instantaneous modulus and the equilibrium modulus as well as the breadth of the viscoelastic relaxation spectrum influence the impact of rate-asymmetry on mechanical efficiency. These insights can be applied to various fields, including soft robotics and bioengineering, which can benefit from efficient elastic mechanisms. By understanding how materials respond to different loading and unloading rates, the design of these systems can be optimized for maximum performance.

5. Material and methods

5.1. Tendons

Bullfrog plantaris tendons were extracted from previously frozen cadavers of the American bullfrog (*Lithobates catesbeianus*). The plantaris muscle-tendon unit was isolated from the tibiafibula. Muscle tissue was then carefully removed from the aponeurosis and tendon. The elastic tissue was kept moist with physiological saline before being frozen again for use in experiments. Previous work has shown that given the low cellular density in tendon, freezing and thawing has no effect on the general mechanical properties of tendons [28,70,71]. All procedures were approved by the University of California, Irvine Animal Care and Use Committee (protocol AUP 20-129).

Guinea fowl common gastrocnemius tendons were extracted from previously frozen cadavers of *Numida meleagris*. The tendon was carefully removed from the insertion point at the tarsometatarsus and the muscle-tendon unit was carefully dissected out and removed from its origin on the femur. Muscle tissue was carefully removed, and the tendon tissue was kept moist with physiological saline before being frozen again to store for later experiments. All procedures were approved by the University of California, Irvine Animal Care and Use Committee (protocol AUP-23-031).

The tendons were removed from the freezer and thawed in a saline solution before being epoxied (J-B Weld WaterWeld Epoxy Putty) between a pair of three-dimensional printed rectangular plates on both ends or clamped between a pair of laser cut acrylic plates with peak-to-peak serrations to prevent slippage [72–74]. The resting length of the tendons was 15 to 22 mm between the printed plates, with a thickness of 0.5 to 1.5 mm. The width of the tendons at the edge of the printed plates was 10 to 20 mm.

5.2. Synthetic elastomers

Prefabricated synthetic elastomer sheets were obtained from McMaster-Carr (polyurethane: catalogue no. 2178T32, thickness 1/32 in, 90A durometer; neoprene: catalogue no. 1370N32, thickness 1/32 in, 60A durometer). These sheets were sectioned into rectangular strips 6 by 40 mm.

5.3. Custom-waveform dynamic mechanical analysis

Using the arbitrary waveform mode of the TA Instruments RSA-G2 DMA, symmetric and asymmetric triangular waves were constructed by superimposing positively sloped and negatively sloped strain versus time lines for the loading and unloading phase respectively. Combinations of five loading times (0.1, 0.316, 1, 3.16 and 10 s) and five unloading times (0.1, 0.316, 1, 3.16 and 10 s) were used to create 25 different loading and unloading combinations. The results in the electronic supplementary material, tables S1 and S2 highlight the loading and unloading time combinations used. The times were chosen to span a difference of two orders of magnitude between the shortest and longest time.

The samples were secured to the tensile clamps of the DMA and a randomized ordering of the 25 different loading and unloading combinations were conducted at approximately 23°C for the selected maximum strain. Three cycles were performed consecutively at a single loading/unloading combination. Between each loading/unloading combination, the samples were allowed to relax 120 s at zero strain to ensure the previous loading history of the material did not affect the results. For the synthetic elastomers, the loading gap with the clamped sample was increased incrementally so that the sample experienced no initial compressive stress. For the tendon samples, approximately 0.05 N of preload force was imposed to reach a sensitive force range that resulted in a final loading gap of approximately 18 mm. A preconditioning protocol of 12 cycles at 3% strain was applied to the tendon samples before testing, consistent with the recommendations of [75]. To keep the tendon samples hydrated, saline solution was applied using a cotton swab during each relaxation period. Because we measured tensile force for thin samples near their equilibrium length, we did not measure any significant negative force due to buckling of the material in response to compression.

The energy input and output for a cycle were computed by numerically integrating the positive area under the stress versus strain curve for the loading and unloading phase respectively. Resilience was calculated by dividing the energy output by the energy input at the third loading and unloading cycle to mitigate transient material response and the Mullins effect [67].

5.4. Modelling the linear viscoelastic resilience of elastomers

To characterize the linear viscoelastic properties of the synthetic polyurethane elastomer, a frequency sweep from 1 to 15 Hz at an oscillation amplitude of 1.0 N was applied to a sample using a TA Instruments Q800 dynamic mechanical analyser. The frequency sweep was first conducted at −40°C and then in increasing temperature increments of 5°C up to 55°C. In the TA Instruments TRIOS software, the TTS functionality was used to shift the storage modulus versus frequency data from all of the temperatures in the experiment to 23°C, the approximate temperature in which the symmetric and asymmetric stretching tests were performed (electronic supplementary material, figure S1). With a focus on the glassy–rubbery transition, the values of storage modulus at the lowest and highest frequency were extended beyond the experimental shifted frequencies to elongate the glassy and rubbery plateau regions. A spline fit interpolation was used to smooth the storage modulus (yellow curve of figure S1c in the electronic supplementary material). The relaxation modulus, $E_{PU}(t)$, for the polyurethane elastomer was obtained from the sine transform of the storage modulus (electronic supplementary material, equation S1).

To model the resilience of elastomers in the linear viscoelastic regime, the generalized Maxwell model consisting of a spring (stiffness E_∞) in parallel with N elements of springs (stiffness E_i) and dashpots (characteristic relaxation time τ_i) in series was used, where $i = 1, \ldots, N$ (figure 3*b*). In the generalized Maxwell model, the relaxation modulus is represented by equation [76]

$$E(t) = E_\infty + \sum_{i=1}^{N} E_i \, e^{-t/\tau_i}. \tag{5.1}$$

For the polyurethane elastomer, E_∞ was obtained from the equilibrium value of $E_{PU}(t)$. To determine the values of E_i and

τ_i, a sum of N exponential decays ($E_i\,e^{-t/\tau_i}$) with equally spaced values for τ_i on the $\log\tau$ scale across the range of times used for the relaxation modulus was fitted to $E_{PU}(t) - E_\infty$ using the Levenberg–Marquardt algorithm (electronic supplementary material, figure S1d). From the sum of squared residuals of the fit across a range of N values, $N = 90$ spring-dashpot elements were chosen from the convergence of the sum of squared residuals for a parsimonious fit (electronic supplementary material, figure S1e). From the values for E_i versus τ_i (representing a discrete relaxation spectrum) and E_∞, the stress response from different loading and unloading combinations was simulated, and the resilience at the third cycle was computed for the polyurethane elastomer (electronic supplementary material, equation S13).

Ethics. All procedures were approved by the University of California, Irvine Animal Care and Use Committee (protocols AUP 20-129 and AUP-23-031).

Data accessibility. All data are included in the manuscript and electronic supplementary material.

Supplementary material is available online [77].

Declaration of AI use. We have not used AI-assisted technologies in creating this article.

Authors' contributions. L.T.: conceptualization, formal analysis, investigation, methodology, software, visualization, writing—original draft, writing—review and editing; P.N.: investigation, validation, writing—review and editing; S.W.: investigation, methodology, writing—review and editing; T.L.: investigation, methodology, writing—review and editing; E.M.: investigation, writing—review and editing; M.J.S.: investigation, writing—review and editing; M.A.D.: conceptualization, resources, writing—review and editing; E.A.: conceptualization, resources, writing—original draft, writing—review and editing; M.I.: conceptualization, resources, supervision, writing—original draft, writing—review and editing.

All authors gave final approval for publication and agreed to be held accountable for the work performed therein.

Conflict of interest declaration. We declare we have no competing interests.

Funding. The authors thank Mikayla Mann for helpful discussions. M.I. acknowledges funding support from the NSF for this work under grant no. 2019371. L.T., P.N., S.W. and T.L. acknowledge funding support from the Harvey Mudd College Physics Summer Research Fund.

References

1. Roberts TJ, Azizi E. 2011 Flexible mechanisms: the diverse roles of biological springs in vertebrate movement. *J. Exp. Biol.* **214**, 353–361. (doi:10.1242/jeb.038588)
2. Higham TE, Irschick DJ. 2013 Springs, steroids, and slingshots: the roles of enhancers and constraints in animal movement. *J. Comp. Physiol. B* **183**, 583–595. (doi:10.1007/s00360-012-0734-z)
3. Ilton M *et al.* 2018 The principles of cascading power limits in small, fast biological and engineered systems. *Science* **360**, aao1082. (doi:10.1126/science.aao1082)
4. Longo SJ, Cox SM, Azizi E, Ilton M, Olberding JP, St Pierre R, Patek SN. 2019 Beyond power amplification: latch-mediated spring actuation is an emerging framework for the study of diverse elastic systems. *J. Exp. Biol.* **222**, 1–10. (doi:10.1242/jeb.197889)
5. Alexander RM, Vernon A. 1975 The mechanics of hopping by kangaroos (Macropodidae). *J. Zool.* **177**, 265–303. (doi:10.1111/j.1469-7998.1975.tb05983.x)
6. Cavagna GA, Heglund NC, Taylor CR. 1977 Mechanical work in terrestrial locomotion: two basic mechanisms for minimizing energy expenditure. *Am. J. Physiol.-Regulat., Integr. Comp. Physiol.* **233**, R243–R261. (doi:10.1152/ajpregu.1977.233.5.R243)
7. Heglund N, Fedak M, Taylor C, Cavagna G. 1982 Energetics and mechanics of terrestrial locomotion. IV. Total mechanical energy changes as a function of speed and body size in birds and mammals. *J. Exp. Biol.* **97**, 57–66. (doi:10.1242/jeb.97.1.57)
8. Dickinson MH, Lighton JR. 1995 Muscle efficiency and elastic storage in the flight motor of *Drosophila*. *Science* **268**, 87–90. (doi:10.1126/science.7701346)
9. Young J, Walker SM, Bomphrey RJ, Taylor GK, Thomas AL. 2009 Details of insect wing design and deformation enhance aerodynamic function and flight efficiency. *Science* **325**, 1549–1552. (doi:10.1126/science.1175928)
10. Fish F, Lauder GV. 2006 Passive and active flow control by swimming fishes and mammals. *Annu. Rev. Fluid Mech.* **38**, 193–224. (doi:10.1146/annurev.fluid.38.050304.092201)
11. Roberts TJ, Abbott EM, Azizi E. 2011 The weak link: do muscle properties determine locomotor performance in frogs? *Phil. Trans. R. Soc. B* **366**, 1488–1495. (doi:10.1098/rstb.2010.0326)
12. Astley HC, Roberts TJ. 2012 Evidence for a vertebrate catapult: elastic energy storage in the plantaris tendon during frog jumping. *Biol. Lett.* **8**, 386–389. (doi:10.1098/rsbl.2011.0982)
13. Burrows M. 2006 Morphology and action of the hind leg joints controlling jumping in froghopper insects. *J. Exp. Biol.* **209**, 4622–4637. (doi:10.1242/jeb.02554)
14. Sutton GP, Burrows M. 2011 Biomechanics of jumping in the flea. *J. Exp. Biol.* **214**, 836–847. (doi:10.1242/jeb.052399)
15. Burrows M, Sutton GP. 2012 Locusts use a composite of resilin and hard cuticle as an energy store for jumping and kicking. *J. Exp. Biol.* **215**, 3501–3512. (doi:10.1242/jeb.071993)
16. Bolmin O, Wei L, Hazel AM, Dunn AC, Wissa A, Alleyne M. 2019 Latching of the click beetle (Coleoptera: Elateridae) thoracic hinge enabled by the morphology and mechanics of conformal structures. *J. Exp. Biol.* **222**, jeb196683. (doi:10.1242/jeb.196683)
17. Patek SN, Korff W, Caldwell RL. 2004 Deadly strike mechanism of a mantis shrimp. *Nature* **428**, 819–820. (doi:10.1038/428819a)
18. Patek S, Rosario M, Taylor J. 2013 Comparative spring mechanics in mantis shrimp. *J. Exp. Biol.* **216**, 1317–1329. (doi:10.1242/jeb.078998)
19. de Groot JH, van Leeuwen JL. 2004 Evidence for an elastic projection mechanism in the chameleon tongue. *Proc. R. Soc. B* **271**, 761–770. (doi:10.1098/rspb.2003.2637)
20. Anderson CV, Sheridan T, Deban SM. 2012 Scaling of the ballistic tongue apparatus in chameleons. *J. Morphol.* **273**, 1214–1226. (doi:10.1002/jmor.20053)
21. Anderson CV. 2016 Off like a shot: scaling of ballistic tongue projection reveals extremely high performance in small chameleons. *Sci. Rep.* **6**, 1–9. (doi:10.1038/srep18625)
22. Patek SN, Baio JE, Fisher BL, Suarez AV. 2006 Multifunctionality and mechanical origins: ballistic jaw propulsion in trap-jaw ants. *Proc. Natl Acad. Sci. USA* **103**, 12 787–12 792. (doi:10.1073/pnas.0604290103)
23. Mendoza E. 2023 Mechanical and physiological determinants of elastic energy storage. PhD thesis, University of California Irvine.
24. Schwaner MJ, Mayfield DL, Azizi M, Daley MA. 2023 Linking *in vivo* muscle dynamics to *in situ* force-length and force-velocity reveals that guinea fowl lateral gastrocnemius operates at shorter than optimal lengths. *bioRxiv*. (doi:10.1101/2023.10.11.561922)
25. Harrison SM, Whitton RC, Kawcak CE, Stover SM, Pandy MG. 2010 Relationship between muscle forces, joint loading and utilization of elastic strain energy in equine locomotion. *J. Exp. Biol.* **213**, 3998–4009. (doi:10.1242/jeb.044545)
26. Gosline JM. 2018 *Mechanical design of structural materials in animals*. Princeton, NJ: Princeton University Press.
27. Mendoza E, Azizi E. 2021 Tuned muscle and spring properties increase elastic energy storage. *J. Exp. Biol.* **224**, jeb243180. (doi:10.1242/jeb.243180)
28. Ker RF. 1981 Dynamic tensile properties of the plantaris tendon of sheep (*Ovis aries*). *J. Exp. Biol.* **93**, 283–302. (doi:10.1242/jeb.93.1.283)
29. Matson A, Konow N, Miller S, Konow PP, Roberts TJ. 2012 Tendon material properties vary and are interdependent among turkey hindlimb muscles. *J. Exp. Biol.* **215**, 3552–3558. (doi:10.1242/jeb.072728)
30. Rosario MV, Roberts TJ. 2020 Loading rate has little influence on tendon fascicle mechanics. *Front. Physiol.* **11**, 255. (doi:10.3389/fphys.2020.00255)
31. Pollock CM, Shadwick RE. 1994 Relationship between body mass and biomechanical properties

of limb tendons in adult mammals. *Am. J. Physiol.-Regul., Integr. Comp. Physiol.* **266**, R1016–R1021. (doi:10.1152/ajpregu.1994.266.3.R1016)

32. Cuming W, Alexander R, Jayes A. 1978 Rebound resilience of tendons in the feet of sheep (*Ovis aries*). *J. Exp. Biol.* **74**, 75–81. (doi:10.1242/jeb.74.1.75)
33. Wold ES, Lynch J, Gravish N, Sponberg S. 2023 Structural damping renders the hawkmoth exoskeleton mechanically insensitive to non-sinusoidal deformations. *J. R. Soc. Interface* **20**, 20230141. (doi:10.1098/rsif.2023.0141)
34. Vermorel R, Vandenberghe N, Villermaux E. 2007 Rubber band recoil. *Proc. R. Soc. A* **463**, 641–658. (doi:10.1098/rspa.2006.1781)
35. Bogoslovov RB, Roland CM. 2007 Viscoelastic effects on the free retraction of rubber. *J. Appl. Phys.* **102**, 063531. (doi:10.1063/1.2784018)
36. Niemczura J, Ravi-Chandar K. 2011 On the response of rubbers at high strain rates: I. Simple waves. *J. Mech. Phys. Solids* **59**, 423–441. (doi:10.1016/j.jmps.2010.09.006)
37. Tunnicliffe LB, Thomas AG, Busfield JJ. 2015 The free retraction of natural rubber: a momentum-based model. *Polym. Test.* **47**, 36–41. (doi:10.1016/j.polymertesting.2015.07.012)
38. Yoon SH, Siviour CR. 2017 Application of the virtual fields method to rubbers under medium strain rate deformation using both acceleration and traction force data. *J. Dyn. Behav. Mater.* **3**, 12–22. (doi:10.1007/s40870-016-0090-2)
39. Ilton M, Cox SM, Egelmeers T, Sutton GP, Patek SN, Crosby AJ. 2019 The effect of size-scale on the kinematics of elastic energy release. *Soft Matter* **15**, 9579–9586. (doi:10.1039/c9sm00870e)
40. Prado RMB, Mishra S, Morgan B, Wijayapala R, Hashemnejad SM, Kundu S. 2020 Achieving high-speed retraction in stretchable hydrogels. *ACS Appl. Mater. Interfaces* **12**, 40719–40727. (doi:10.1021/acsami.0c08132)
41. Liang X, Crosby AJ. 2020 Programming impulsive deformation with mechanical metamaterials. *Phys. Rev. Lett.* **125**, 108002. (doi:10.1103/PhysRevLett.125.108002)
42. Liang X, Crosby AJ. 2022 Dynamic recoil in metamaterials with nonlinear interactions. *J. Mech. Phys. Solids* **162**, 104834. (doi:10.1016/j.jmps.2022.104834)
43. Chi Y, Hong Y, Zhao Y, Li Y, Yin J. 2022 Snapping for high-speed and high-efficient butterfly stroke–like soft swimmer. *Sci. Adv.* **8**, eadd3788. (doi:10.1126/sciadv.add3788)
44. Kim S, Hsiao YH, Lee Y, Zhu W, Ren Z, Niroui F, Chen Y. 2023 Laser-assisted failure recovery for dielectric elastomer actuators in aerial robots. *Sci. Robotics* **8**, eadf4278. (doi:10.1126/scirobotics.adf4278)
45. Burrows M, Shaw SR, Sutton GP. 2008 Resilin and chitinous cuticle form a composite structure for energy storage in jumping by froghopper insects. *BMC Biol.* **6**, 1–16. (doi:10.1186/1741-7007-6-41)
46. Patek S, Dudek D, Rosario M. 2011 From bouncy legs to poisoned arrows: elastic movements in invertebrates. *J. Exp. Biol.* **214**, 1973–1980. (doi:10.1242/jeb.038596)
47. Bao G, Suresh S. 2003 Cell and molecular mechanics of biological materials. *Nat. Mater.* **2**, 715–725. (doi:10.1038/nmat1001)
48. Buehler MJ. 2007 Nano- and micromechanical properties of hierarchical biological materials and tissues. *J. Mater. Sci.* **42**, 8765–8770. (doi:10.1007/s10853-007-1952-8)
49. Fung Y. 2013 *Biomechanics: mechanical properties of living tissues*. New York, NY: Springer Science & Business Media.
50. Tang S, Richardson BM, Anseth KS. 2021 Dynamic covalent hydrogels as biomaterials to mimic the viscoelasticity of soft tissues. *Prog. Mater. Sci.* **120**, 100738. (doi:10.1016/j.pmatsci.2020.100738)
51. Shearer T, Thorpe CT, Screen HR. 2017 The relative compliance of energy-storing tendons may be due to the helical fibril arrangement of their fascicles. *J. R. Soc. Interface* **14**, 20170261. (doi:10.1098/rsif.2017.0261)
52. Anderson PS, Kawano SM. 2022 Different traits at different rates: the effects of dynamic strain rate on structural traits in biology. *Integr. Comp. Biol.* **62**, 683–699. (doi:10.1093/icb/icac066)
53. Azizi E, Roberts TJ. 2009 Biaxial strain and variable stiffness in aponeuroses. *J. Physiol.* **587**, 4309–4318. (doi:10.1113/jphysiol.2009.173690)
54. Abdala V, Ponssa ML, Tulli MJ, Fabre AC, Herrel A. 2018 Frog tendon structure and its relationship with locomotor modes. *J. Morphol.* **279**, 895–903. (doi:10.1002/jmor.20819)
55. Lieber RL, Leonard ME, Brown CG, Trestik CL. 1991 Frog semitendinosis tendon load-strain and stress-strain properties during passive loading. *Am. J. Physiol.-Cell Physiol.* **261**, C86–C92. (doi:10.1152/ajpcell.1991.261.1.C86)
56. Patek S. 2019 The power of mantis shrimp strikes: interdisciplinary impacts of an extreme cascade of energy release. *Integr. Comp. Biol.* **59**, 1573–1585. (doi:10.1093/icb/icz127)
57. Griffiths R. 1991 Shortening of muscle fibres during stretch of the active cat medial gastrocnemius muscle: the role of tendon compliance. *J. Physiol.* **436**, 219–236. (doi:10.1113/jphysiol.1991.sp018547)
58. Reeves ND, Narici MV. 2003 Behavior of human muscle fascicles during shortening and lengthening contractions in vivo. *J. Appl. Physiol.* **95**, 1090–1096. (doi:10.1152/japplphysiol.01046.2002)
59. Dudek DM, Full RJ. 2006 Passive mechanical properties of legs from running insects. *J. Exp. Biol.* **209**, 1502–1515. (doi:10.1242/jeb.02146)
60. Daley MA, Biewener AA. 2003 Muscle force-length dynamics during level versus incline locomotion: a comparison of *in vivo* performance of two guinea fowl ankle extensors. *J. Exp. Biol.* **206**, 2941–2958. (doi:10.1242/jeb.00503)
61. Birn-Jeffery AV, Hubicki CM, Blum Y, Renjewski D, Hurst JW, Daley MA. 2014 Don't break a leg: running birds from quail to ostrich prioritise leg safety and economy on uneven terrain. *J. Exp. Biol.* **217**, 3786–3796. (doi:10.1242/jeb.102640)
62. Clemente CJ, Bishop P, Newman N, Hocknull S. 2018 Steady bipedal locomotion with a forward situated whole-body centre of mass: the potential importance of temporally asymmetric ground reaction forces. *J. Zool.* **304**, 193–201. (doi:10.1111/jzo.12521)
63. Nilsson J, Thorstensson A. 1989 Ground reaction forces at different speeds of human walking and running. *Acta Physiol. Scand.* **136**, 217–227. (doi:10.1111/j.1748-1716.1989.tb08655.x)
64. Cavagna GA. 2010 Symmetry and asymmetry in bouncing gaits. *Symmetry* **2**, 1270–1321. (doi:10.3390/sym2031270)
65. Rebula JR, Kuo AD. 2015 The cost of leg forces in bipedal locomotion: a simple optimization study. *PLoS ONE* **10**, e0117384. (doi:10.1371/journal.pone.0117384)
66. Polet DT, Bertram JE. 2019 An inelastic quadrupedal model discovers four-beat walking, two-beat running, and pseudo-elastic actuation as energetically optimal. *PLoS Comput. Biol.* **15**, e1007444. (doi:10.1371/journal.pcbi.1007444)
67. Cheng M, Chen W, Weerasooriya T. 2009 Mechanical behavior of bovine tendon with stress-softening and loading-rate effects. *Adv. Theor. Appl. Mech.* **2**, 59–74.
68. Bennet-Clark H. 1975 Scale effects in jumping animals. In *Scale effects in animal locomotion* (ed. TJ Pedley), pp. 185–200. London, UK: Academic Press.
69. Challita EJ, Alexander SL, Han SI, Blackledge TA, Coddington JA, Jung S, Bhamla MS. 2021 Slingshot spiders build tensed, underdamped webs for ultrafast launches and speedy halts. *J. Comp. Physiol. A* **207**, 205–217. (doi:10.1007/s00359-021-01475-5)
70. Chen L, Wu Y, Yu J, Jiao Z, Ao Y, Yu C, Wang J, Cui G. 2011 Effect of repeated freezing–thawing on the Achilles tendon of rabbits. *Knee Surg. Sports Traumatol. Arthrosc.* **19**, 1028–1034. (doi:10.1007/s00167-010-1278-y)
71. Lee AH, Elliott DM. 2017 Freezing does not alter multiscale tendon mechanics and damage mechanisms in tension. *Ann. N Y Acad. Sci.* **1409**, 85–94. (doi:10.1111/nyas.13460)
72. Shi D, Wang D, Wang C, Liu A. 2012 A novel, inexpensive and easy to use tendon clamp for in vitro biomechanical testing. *Med. Eng. Phys.* **34**, 516–520. (doi:10.1016/j.medengphy.2011.11.019)
73. Cheung JTM, Zhang M. 2006 A serrated jaw clamp for tendon gripping. *Med. Eng. Phys.* **28**, 379–382.
74. Jiang M, Lawson ZT, Erel V, Pervere S, Nan T, Robbins AB, Feed AD, Moreno MR. 2020 Clamping soft biologic tissues for uniaxial tensile testing: a brief survey of current methods and development of a novel clamping mechanism. *J. Mech. Behav. Biomed. Mater.* **103**, 103503. (doi:10.1016/j.jmbbm.2019.103503)
75. Ebrahimi M, Mohammadi A, Ristaniemi A, Stenroth L, Korhonen RK. 2019 The effect of different preconditioning protocols on repeatability of bovine ACL stress-relaxation response in tension. *J. Mech. Behav. Biomed. Mater.* **90**, 493–501. (doi:10.1016/j.jmbbm.2018.10.041)
76. Tschoegl NW. 2012 *The phenomenological theory of linear viscoelastic behavior: an introduction*. Berlin, Germany: Springer Science & Business Media.
77. Tsai L, Navarro P, Wu S, Levinson T, Mendoza E, Janneke Schwaner M, Daley MA, Azizi E, Ilton M. 2024 Viscoelastic materials are most energy efficient when loaded and unloaded at equal rates. Figshare. (doi:10.6084/m9.figshare.c.7029148)